

# EXTENDED SOURCE ANALYSIS FOR GRATING SPECTROMETERS

D. Dewey <sup>a</sup>

<sup>a</sup>MIT Center for Space Research, Cambridge MA 02139, USA

Dispersive spectrometers such as the *XMM-Newton* RGS and the *Chandra* HETGS/LETGS are nominally designed and used to study “point sources”, that is sources unresolved by the telescope system. When used to observe “extended sources” the resolving power of these spectrometers is generally degraded; however, useful high-resolution information may still be extracted using non-standard analysis techniques. Which technique to use and the amount of information extractable from an observation depend on the spatial and spectral properties of the object. Examples are given of “spatial-spectral” techniques that are in development, in particular ones being used to extract high-resolution results from *Chandra* HETGS observations of the supernova remnants E0102, N132D, N103B, and Cas A.

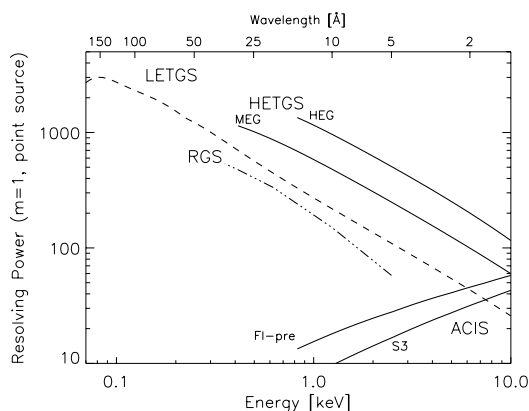


Figure 1. Spectrometers’ resolving powers when observing point sources.

## 1. Spectrometers and Extended Sources

The *Chandra* and *XMM-Newton* gratings provide high resolving power over a large wavelength range as plotted in Fig. 1. Also plotted are values for ACIS CCDs: the FI devices before CTI degradation and the BI S3 chip.

The high spectral resolution of the grating spectrometers is due to the combination of a telescope (mirror/detector) system with small spatial resolution and gratings with high grating dispersion, *e.g.*, see Figure 1 of Canizares(2000)[1].

The response to a monochromatic line is given

as a starting point by the zeroth-order image. Grating effects will cause dispersed images to differ from the zeroth-order image. For HEG and MEG there is a slight additional dispersion blurring and few arc second cross-dispersion spreading. For LETG there is also the coarse and fine support structure effects which differ in zeroth and dispersed orders. For the RGS the reflection gratings add additional PSF and scatter effects. Also for the RGS, the aspect ratio of the image is not preserved and varies with the wavelength scale.

### 1.1. Effect of Source Size w/E0102

The *Chandra* HETG observation of E0102 is a good example of the effect of observing an extended source. Using essentially standard processing with an increased cross-dispersion spatial extraction region, a spectrum (*pha* file) is created for the MEG minus-first order, shown by the orange curve in Fig. 2. A monochromatic line, like the 19 Å Oxygen VIII Lyman alpha line, has a response in the spectrum that is broadened from what a point source would produce. If an *rmf* file is created that encodes this broadening (more below) then it is possible to do the usual forward folding fitting, *e.g.*, with XSPEC models in ISIS[2]. For example a single *vnpshock\*wabs* model (purple) roughly fits these E0102 MEG data; this model is also shown as it would appear for the case of a point source with standard MEG resolution (green).

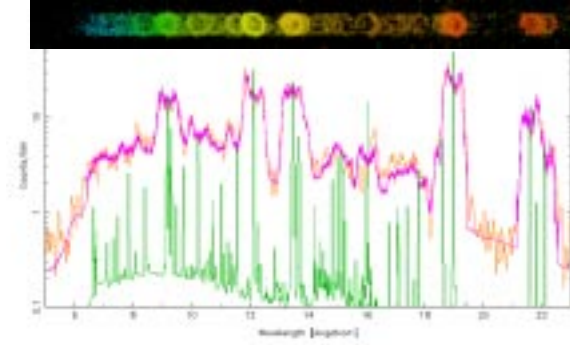


Figure 2. Dispersed image and spectrum of E0102 as observed with the MEG grating on *Chandra*. The ring-like image of the SNR is visible in the individual dispersed line images. The resulting histogram (orange) has a resolving power significantly degraded compared to the case of a point source line response (green.)

## 1.2. Resolving Power Equations

The grating spectrometers' resolution performance (in first order) can be summarized by a few parameters, given in Table 1 below. Using these values the spectrometer resolution is approximated by the RSS sum of telescope, grating, and extended source terms. Specifically in IDL we have:

$$d\_lambda = \text{SQRT}((\text{aperas} * \text{imgfwhm})^2 + (2.35 * \text{dpp} * \text{lambda})^2 + (\text{aperas} * \text{objsize})^2)$$

and

$$\text{Resolving\_power} = \text{lambda} / d\_lambda$$

The value *aperas* is the sensitivity of spectral blur to the source size in units of "Å per arc sec". For these instruments this value is determined by the effective period, focal length and Rowland spacing as  $p_{\text{eff}} * (fl/R_s)$  with units of Å/radian.

Table 1  
Grating Spectrometer Parameters (approximate)

Grating	$p_{\text{eff}}$ , Å	<i>aperas</i>	<i>imgfwhm</i>	<i>dpp</i>
RGS1	425	0.00232	24.8"	510e-6
HEG	2000	0.0111	0.80"	146e-6
MEG	4000	0.0222	0.88"	235e-6
LEG	10000	0.0555	0.80"	100e-6

For RGS  $p_{\text{eff}}$  is the product of the physical spacing, 645.6 l/mm or 15,500 Å, times the sine of the incident graze angle,  $\alpha \approx 1.57$  degrees. *imgfwhm* and *objsize* are the total image blur and object size, in arc seconds FWHM. *dpp* is the rms period variation within and between the grating components and causes a slight reduction of resolving power at longer wavelengths.

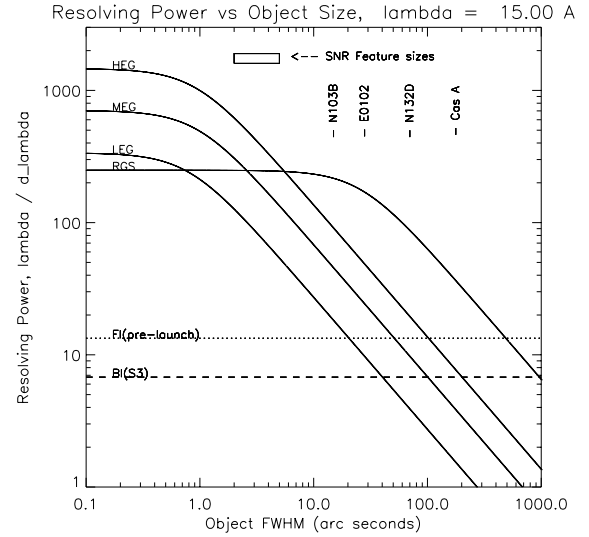


Figure 3. Resolving power at 15 Å versus extended source size (FWHM).

Fig. 3 shows the grating resolving powers from the previous equations plotted as a function of the object size (FWHM) in the dispersion direction. Note at small sizes the *Chandra* spectrometers have higher resolving power but there is a cross-over where they fall below the RGS value, at about 0.75, 2.5, and 5.5 arc seconds for LEG, MEG, and HEG respectively. At greater sizes the RGS resolving power also decreases and there is a fixed relation between them as they all vary as  $1/\text{size}$ .

## 2. SNRs in HETG GTO Program

*Chandra* has produced detailed images of SNR[3]; four of these have been observed in the HETG GTO program, shown to the same scale in Fig. 4. N103B shows strong Si lines and a bright

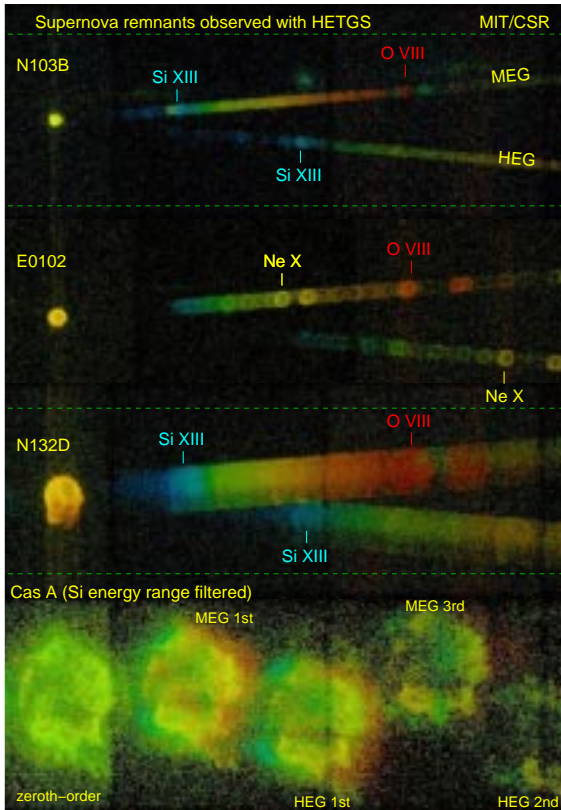


Figure 4. Supernova remnants as observed in the HETG GTO program are shown on the same scale.

Fe forest from 7 to 18 Å. E0102 shows a clear ring structure with bright lines of O, Ne, Mg and very little Fe. N132D shows prominent O and Fe lines as well as Ne, Mg, and Si; its image consists of many filaments as narrow as 2 to 5 arc seconds. Cas A is cutoff with strong Si and S lines and structure on small scales (see below); in Fig. 4 the Cas A dispersed image is only of events in the Si XIII-XIV energy range. The rough sizes of these SNRs are indicated on Fig. 3. Clearly these remnants are large for *Chandra* grating observations, however the SNRs do show spatial features on a small scale of 2 to 5 arc seconds. From an analysis point of view each SNR may be considered a set of sources in a single complex field.

### 3. 1-D Analysis Approaches

As a first cut for extended source analysis it is useful to explore what can be done using the 1-dimensional machinery that is already available, that is forward folding spectral models through `arf` and `rmf` files to find best fits to `pha` files created from the data. This implicitly assumes a spectrum which is independent of spatial coordinates; significant spatial-spectral effects can be uncovered by looking for systematic residuals in the 1-D approach.

One or more `pha` files can be created with standard analysis s/w choosing appropriate cross-dispersion regions and assuming that order-sorting of events is possible. For relatively small objects the full object may be captured in a single `pha` file as in the case of N103B below. The cross-dispersion region may be set to extract just a specific feature or bright filament, see Cas A example below. Or a quasi-two-dimensional analysis can be carried out by slicing the object into multiple cross-dispersion regions as in Fig. 5 and simultaneously fitting a single spectral model to the set of `pha` files that are created.

For the 1-D analysis it is necessary to generate `arf` and `rmf` files that go along with the extracted `pha` file(s). If the response varies little over the size of the source then an `arf` file for a point source at an appropriate location can be a good approximation.

Creation of `rmf` files is the most novel part of these 1-D approaches. For RGS observations, a model in XSPEC 11.2, `rgsxsrsc`, can generate an `rmf` based on an input image, taking into account the main effect of the extended source on the spectrum; alternatively `rgsrmfgen` may be used[4]. For our *Chandra* observations, custom

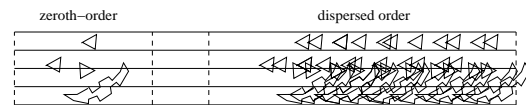


Figure 5. In a quasi-2D approach multiple 1-D spectra are extracted from a dispersed 2-D object and analyzed simultaneously with conventional s/w (ISIS, XSPEC,...). More information is retained than if a single large extraction region were used.

“filament analysis” s/w written in IDL extracts the `pha` file(s) and uses the zeroth-order events to create matching `rmf` file(s) in which the response at a given energy is based on the ACIS ENERGY-filtered events. Note that in these methods chip gap regions are not accurately modelled in the response and so should be ignored.

### 3.1. N103B: `rmf`'s with Spatial Information

The HETG observation of N103B had dispersion roughly along the E-W direction; the bright western side has a width of about  $16''$  or  $0.35 \text{ \AA}$  in the MEG. The extracted spectrum is shown in Fig. 6 and fitting was done in ISIS using an `rmf` created with our filament s/w. Single-ion spectral models[5] are useful for fitting this intermediate-resolution spectrum and remove ionization balance from the model. Element abundances depend on the assumed model and using the single-ion values, Fig. 7, does not include X-ray-invisible plasma, e.g. O VI. This modeling shows that the *required* amounts of O and Ne may be well below standard NEI or shock model estimates[8,9].

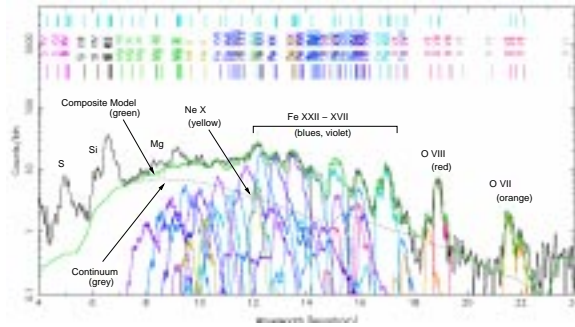


Figure 6. The MEG minus-order spectrum (1-D `pha`) from N103B is shown fit by a composite model. Each model component is the line emission from a single ion. There is sufficient resolution in the spectrum for the main line of many ions to stand out clearly like the tip of an iceberg.

### 3.2. CasA: “Filament Analysis”

A special but useful case motivated by N132D[10] and applied here to CasA is “filament analysis”. A bright filament can be “straightened” to lie along the cross-dispersion axis by defining

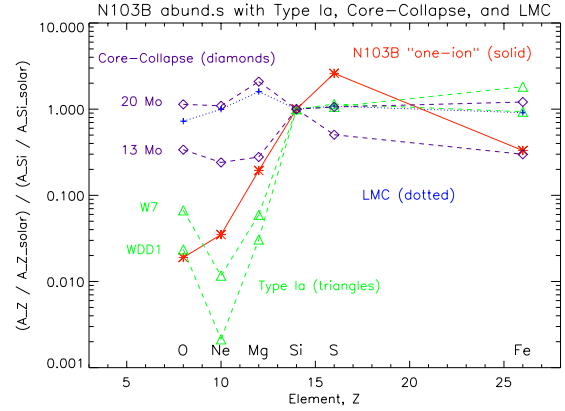


Figure 7. The abundances of elements in N103B relative to Si are compared with LMC abundances and yields of Type Ia[6] and core-collapse[7] models. The “one-ion” values are based only on X-ray visible plasma and hence are lower limits.

a “path” which is used as a lookup table to adjust zeroth-order and dispersed events; see Fig. 8. This enhances the sensitivity to emission lines from spatially narrow 1-D features. Note that the continuum under lines may have contributions from many spatial regions and is best measured for a filament using the undispersed image.

Spectra were extracted for the “Si South” region of Cas A, Fig. 8. The line fluxes and an overall blue-shift were fit in ISIS by fixing the relative line spacings and the  $i/f$  ratio for the Si XIII triplet.

## 4. 2-D Spatial-Spectral Analysis

When true spatial-spectral variation exists in the source it is necessary to use more than simple 1-D techniques[15]. The overlapping of spectral images in the dispersed image represents a loss of information. However the combination of a sparse spatial image,  $\beta_{xy} < 1$ , and a sparse emission spectrum,  $\beta_\lambda < 1$ , reduces overlap, Fig. 9; the  $\beta$ s are spectral and spatial sparsity (filling) factors.

In general the source has  $n \times n$  spatial resolution cells and  $l$  wavelength resolution cells for a total of  $n^2 l$  degrees of freedom. Each dispersed image from a single grating/order spectrum contains  $n \times l$  measurements. In order to have the number of measurements be greater than unknowns

we need  $N_s$  spectra so that  $N_s \geq \beta_\lambda \beta_{xy} n$ . Note that the width or sharpness of bright features is an additional image parameter and determines the minimum wavelength or velocity resolution for the data set.

As an example of a full 2-D analysis, the Ne X line in E0102 was modelled using the machinery of Fig. 9. A 3-D spatial-velocity data cube represents the truth about the source and is forward folded through the instrument response to create 2-D plus/minus dispersed images that are compared with the measured data. After conjugate-gradient iteration to reduce the figure of merit (the sum of  $\chi^2$  and an entropy term), the resulting best fit data cube is used to produce a spatial-velocity image of the Ne X line, Fig. 10, similar to narrow-band Fabry-Perot imaging. This image strongly suggests a cylinder-like geometry.

## REFERENCES

1. Canizares, C. R. *et al.* 2000, ApJ, 539L, 41.
2. Houck, J. C., these proceedings.
3. Chandra Supernova Remnant Catalog, <http://hea-www.harvard.edu/ChandraSNR/>.
4. Ballet, J., these proceedings.
5. Wojdowski, P. S., these proceedings.
6. Iwamoto, K. *et al.* 1999, ApJSS, 125, 439.
7. Thielemann, F-K. *et al.* 1996, ApJ, 460, 408.
8. Migliazzo, J. *et al.* 2002, APS meeting, 47, N17.039.
9. van der Heyden, K. J., *et al.* 2002, A&A, 392, 955; and these proceedings.
10. Canizares, C. R. *et al.* 2001, in “Young supernova remnants”, eds Holt, S. S., & Hwang, U., AIP Conf. Proc., 565, 213.
11. Markert, T. H. *et al.* 2000, ApJ, 268, 13.
12. Holt, S. S. *et al.* 1994, PASJ, 46, L151.
13. Hwang, U. *et al.* 2001, ApJ, 560, L175.
14. Willingale, R. *et al.* 2002, A&A, 381, 1039.
15. Peterson, J. R. *et al.*, these proceedings.
16. Flanagan, K. A. *et al.* 2003, in preparation.

## ACKNOWLEDGEMENTS

I’d like to express gratitude to Claude Canizares for the privilege of working on the HETG and to the HETG and CXC group members at the CSR for so much and varied support. Specific contributions to this work were made by Kathryn Flanagan, Amy Fredericks, John Houck, Josh Migliazzo, and Patrick Wojdowski. This work was supported by NASA through contracts NAS8-38249 and NAS8-01129.

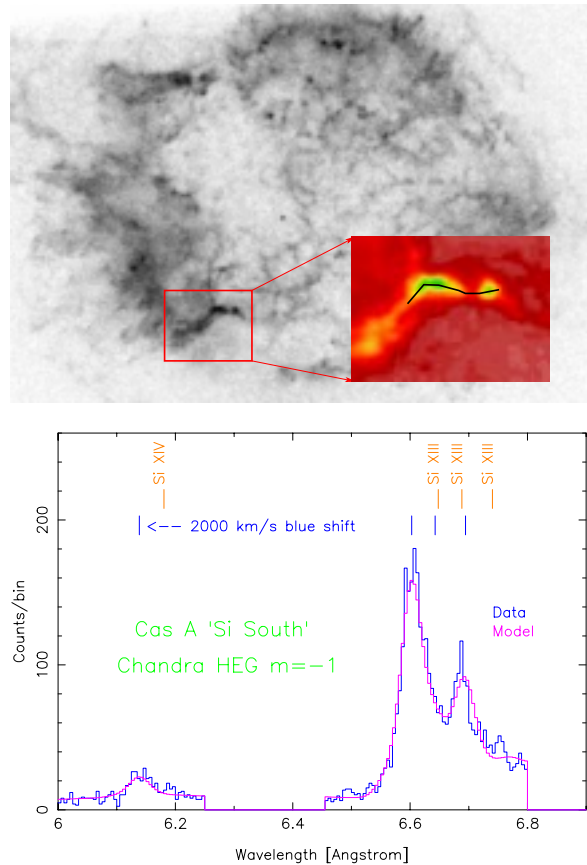


Figure 8. **Upper image:** Cas A filtered on Si emission with the bright “Si South” feature enclosed in the rectangle; the dispersion axis is roughly vertical. The “filament path” for this feature is indicated on the expanded color-intensity plot, inset. **Lower plot:** The HEG spectrum from this feature is fit by a constrained 4-line model. A blue-shift of  $\approx 2000$  km/s is clearly measured in agreement with Einstein/FPCS[11], ASCA[12], ACIS[13], and EPIC-MOS[14] results. The Si line ratios constrain an NEI model of this feature to  $\log_{10}(n_e t) > 11$  and  $\log_{10}(T) \approx 7.0 \pm 0.2$ .

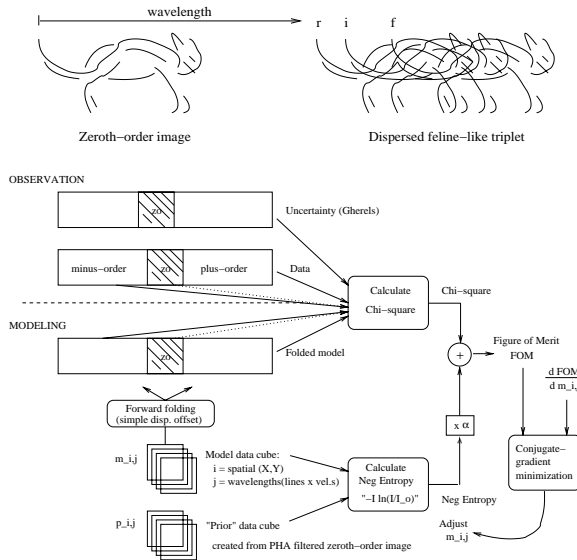


Figure 9. 2-D spatial-spectral approach. The **top schematic** shows a sparse, spatially complex 2-D object at left and the resulting dispersed image for the spectrally sparse case of only three emission lines. Note the minimal overlap (intersections) among the three individual spectral images which preserves the spatial-spectral information. The **lower block diagram** summarizes one implementation of a full 2-D spatial-spectral forward folding scheme used to extract source images in discrete wavelength (velocity) planes from dispersed data. The figure of merit being minimized includes an entropy term which measures the deviation of the modelled image planes from priors based on the zeroth-order image.

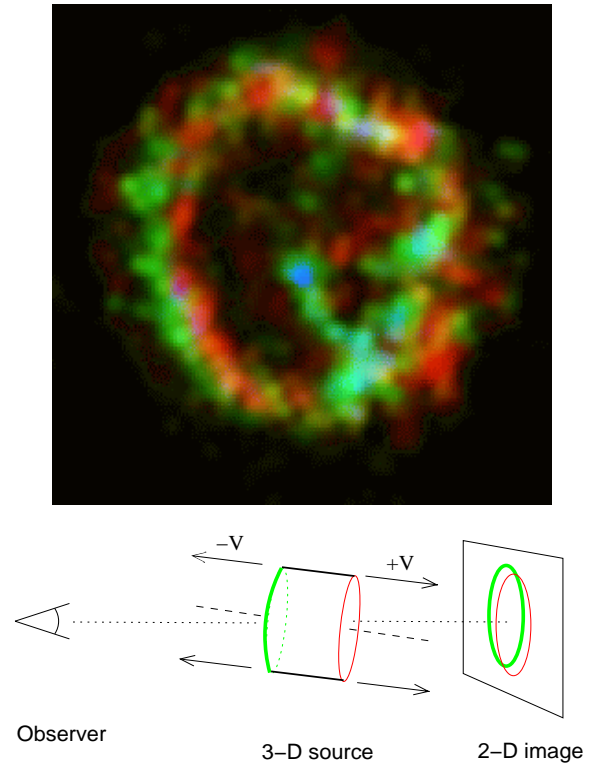


Figure 10. Spatial-velocity structure of Ne X line emission from E0102. The **top image** shows the spatial-velocity result of fitting the Ne X dispersed data with a source model consisting of images in 5 wavelengths, corresponding to velocity offsets (and corresponding color code) of +1800 and +900 km/s (red), 0 km/s (not coded), -900 km/s (green), and -1800 km/s (blue), from [16]. The **lower diagram** shows how roughly cylindrical motion viewed slightly off axis can lead to the observed spatial offset of velocity components.